Journal of the Korean Physical Society, Vol. 42, February 2003, pp. S893∼S899

Numerical Computation on the Generation of CH_3 and H Radicals by the Thermal Plasma Decomposition of Hydrocarbons

Keun Su Kim,* Tae Hyung Hwang, Su Seok Choi and Sang Hee Hong
Department of Nuclear Engineering, Seoul National University, Seoul 157-742

Homin Shin
Korea Accelerator and Plasma Research Association, Gangwon-do 269-843

A two-dimensional numerical analysis on the thermal decomposition of methane (CH_4) by Ar/H_2 thermal plasmas has been carried out using a FLUENT code to find out the effects of thermal plasma fields on the production rates of CH_3 and H radicals during the CH_4 decomposition process in a dc arc-jet diamond CVD. In the numerical analysis, the partial differential equations describing conservations of mass, momentum, and energy as well as mass of individual chemical species are taken into account along with the $K-\epsilon$ turbulence model. The numerical calculations are performed in the following consecutive procedure. In the first step, the thermal plasma fields inside a reaction chamber are calculated from the inlet boundary conditions without considering chemical reactions. Uniform profiles of the plasma temperature and velocity at the torch exit are assumed as the inlet boundary conditions in this step. Next in the second calculation step, the chemical kinetic equations, involving 13 species and 25 reactions, are solved in the environment of the calculated two-dimensional plasma fields to give the concentration fields of all chemical species generated in the CH_4 decomposition process. The calculated results show that the developed plasma fields inside the reaction chamber strongly depend on the reaction chamber geometry, and significantly affect the concentration fields and generation rates of the decomposed radicals, such as CH_3 and H.

PACS numbers: 52.30.-q, 02.60.-x
Keywords: dc arc-jet diamond CVD, numerical modeling, two-dimensional, thermal plasma decomposition, radicals generation

I. INTRODUCTION

Recently, thermal plasmas produced by dc plasma torches have provided effective means for the generation of CH_3 and H radicals through the thermal decomposition of hydrocarbons due to their high temperature and high energy density. In this connection, there have been considerable attempts to synthesize diamond films by the thermal plasma decomposition of hydrocarbons [1–3]. In an effort to optimize the thermal plasma diamond CVD process, many research groups have studied the fundamental processes involved with the thermal plasma decomposition of hydrocarbons and developed several numerical models of the gas-phase chemistry in C/H/Ar gas mixtures. For example, a plug-flow reactor model [4], based on the estimated temperature and residence time profiles, has been widely used for improving the diamond film deposition process, and has given useful information on the thermal plasma decomposition mechanism of hydrocarbons.

In the material processing with thermal plasmas, it is generally known that plasma fields established inside reaction chambers by thermal plasma torches have considerable effects on the overall quality of the process products [5–7]. Thus, scientific and technical information on the effects of plasma fields, which strongly depend on the chamber geometry and operation conditions, is necessary to predict process performances accurately and realize optimizations of thermal plasma processes. However, until now most of numerical analysis on the thermal plasma diamond CVD have relied on the one-dimensional (1D) plug-flow reactor model, and it has been impossible to take into account phenomena such as re-circulating flows at the torch exit, mixing effects of reaction gases near a hydrocarbon injection tube, and radial transports of chemical species. These phenomena are crucial for the actual process optimizations, and must be taken into account in the development of numerical models of the thermal plasma diamond CVD for proper calculations of concentration fields. Therefore, a two-dimensional (2D) numerical approach to the gas-phase chemistry in the thermal plasma diamond CVD is essentially necessary to obtain a more accurate and complete picture of the chemical reactions occurring in the reaction chamber.

In this work, a 2D numerical analysis on the thermal

*E-mail: nuclear@snu.ac.kr

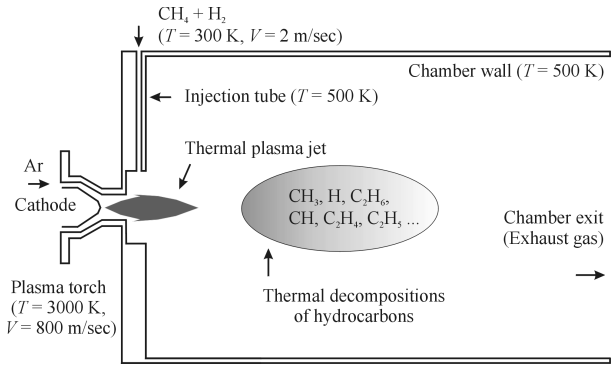

Fig. 1. Schematic diagram of a dc arc-jet diamond CVD process.

decomposition of CH_4 by Ar/H_2 thermal plasmas has been carried out using the FLUENT code to find out the effects of plasma fields, *i.e.*, temperature profiles and flow patterns, on the production rates of CH_3 and H radicals during the CH_4 decomposition process. A set of coupled partial differential equations for finding concentration fields of chemical species is numerically solved using the control volume method suggested by Patankar [8]. In the numerical calculations, 13 species and 25 chemical reaction mechanisms are taken into account to obtain reasonable calculation results and avoid numerical instabilities in the computation. The 2D concentration fields of major radicals, such as CH_3 and H, are then obtained so that the effects of plasma fields on the radicals generation might be investigated.

II. NUMERICAL MODELING

A schematic diagram of a dc arc-jet diamond CVD process considered in the present study is depicted in Fig. 1. A non-transferred dc plasma torch is used as an arc-jet flame generator of argon plasma, and reaction gases of CH_4 and H_2 are radially injected through an injection tube into the argon plasma jet for the CH_3 and H radicals generation. The geometrical and operational conditions of the dc arc-jet diamond CVD system are summarized in Table 1.

1. Fluid dynamic equations

The partial differential equations describing conservations of mass, momentum, and energy are considered along with the standard $K-\epsilon$ turbulence model to calculate plasma fields in the two dimensions, for which an axisymmetric assumption is employed due to a cylindrical geometry of the system. The standard wall function approach is used for the near-wall treatments.

Table 1. Geometrical and operational conditions of the dc arc-jet diamond CVD system described in Fig. 1.

Geometrical Conditions	Torch diameter	10 mm
	Injection tube diameter	1 mm
	Reaction chamber diameter	50 mm
	Reaction chamber length	250 mm
Operational Conditions	Arc gas	Ar
	Reaction gas	CH_4/H_2(5/95 %)
	Inlet velocity of reaction gas	2 m/s
	Chamber pressure	1 atm

To define a composition-dependent mass density of a mixture gas in the thermal plasma, the mixture is assumed to be an ideal incompressible gas, and its mass density ρ is computed from

$$\rho = \frac{P}{RT\sum_s \frac{m_s}{M_s}} \tag{1}$$

where R is the universal gas constant, T is the plasma temperature, m_s is the mass fraction of species s, M_s is the molecular weight of species s, and P is the operating pressure. And the physical properties of the mixture gas, such as viscosity and thermal conductivity, are computed simply based on the mass fraction average of its constituent pure species properties. For example, the viscosity of the mixture is defined by

$$\mu = \sum_s m_s \mu_s \tag{2}$$

where μ_s is the viscosity of species s.

2. Species transport equations

The conservation equations for individual chemical species have the following form:

$$\frac{\partial}{\partial x_i}(\rho u_i m_s) = -\frac{\partial}{\partial x_i} J_{s,i} + R_s \tag{3}$$

where u_i is the velocity in the i direction, R_s is the mass rate of creation or depletion by chemical reactions, and $J_{s,i}$ is the diffusion flux of species s. The source R_s of chemical species s due to the reaction is computed as the sum of the reaction sources over the N_R reactions that the species may participate in:

$$R_s = M_s \sum_{k=1}^{N_R} \hat{R}_{s,k} \tag{4}$$

where $\hat{R}_{s,k}$ is the molar rate of creation and destruction of species s in reaction k. The molar rate of creation and destruction of species s in reaction k is given by [9]

$$\hat{R}_{s,k} = \sum_{s'=1}^{N} \alpha_{s'k}[C_{s'}](k_{f,k} \prod_{s'=1}^{N} [C_{s'}]^{\eta_{s',k}} - k_{b,k} \prod_{s'=1}^{N} [C_{s'}]^{\eta'_{s',k}}) \quad (5)$$

where N is the total number of chemical species, $\alpha_{s'k}$ is the third-body efficiency of the s'th species in reaction k, $k_{f,k}$ is the forward rate constant for reaction k, $k_{b,k}$ is the backward rate constant for reaction k, $C_{s'}$ is the molar concentration of each reactant or product species s', $\eta_{s',k}$ is the reaction order for reactant s' in reaction k, and $\eta'_{s',k}$ is the reaction order for product s' in reaction k. Since proper data for the reaction orders are not available for the time being, the stoichiometric coefficients for each reaction are used as the corresponding reaction orders. In addition, it is also assumed that all species in the mixture contribute equally as the third bodies, *i.e.*, $\alpha_{s'k}$ = 1, however, it is often the case that some species act more efficiently as the third bodies than do others [9].

In turbulent flows, mass diffusion terms are computed in the following form:

$$J_{s,i} = -(\rho D_{s,m} + \frac{\mu_t}{S_{ct}}) \frac{\partial m_s}{\partial x_i} \quad (6)$$

where μ_t is the turbulent viscosity, $D_{s,m}$ is the diffusion coefficient of species s in the mixture, and S_{ct} is the turbulent Schmidt number. Unfortunately, the reliable diffusion coefficient data for the all species considered in this work are limited, thus a constant dilute-approximation scheme is employed for the actual calculations of diffusion terms.

3. Reaction mechanism

The gas-phase reaction mechanism considered in this work consists of 25 chemical reactions listed in Table 2, in which M denotes third body molecules. Rate constants for the each reaction are obtained from the combustion literatures [10–14], and the temperature dependency of a forward reaction rate constant $k_{f,k}$ for reaction k is expressed in the Arrhenius form,

$$k_{f,k} = A_k T^{nk} \exp(-E_{ak}/RT) \quad (7)$$

where A_k is the pre-exponential factor, n_k is the temperature exponent, and E_{ak} is the activation energy for reaction k. Each reaction is reversible, and a backward rate constant $k_{b,k}$ for reaction k is computed from the reaction equilibrium constant using the following relation:

$$k_{b,k} = k_{f,k}/K_k \quad (8)$$

where K_k is the equilibrium constant for reaction k. Finally, thermodynamic properties for the individual species, such as heat capacity, standard state enthalpy, and standard state entropy, are taken from NIST (National Institute of Standards and Technology) thermodynamic database and combustion literatures. Owing to the lack of reliable data at high temperatures, the rate constants are used over the recommended temperature range, and most of the thermodynamic data are linearly extrapolated from the lower temperature data. In addition, all surface reactions on the reaction chamber wall are neglected in this numerical work.

4. Boundary conditions

The following boundary conditions are used for finding the unique solutions of the plasma and concentration fields.

A. Boundary conditions for fluid dynamic equations

i) The no-slip conditions are assumed on the reaction chamber wall and the wall temperature is given as 500 K.

ii) The symmetry conditions (*i.e.*, no gradient in the radial direction) are imposed at the symmetric axis.

iii) It is assumed that the plasma temperature and velocity at the torch exit have uniform distributions of 3000 K and 800 m/sec, respectively.

iv) The temperature and velocity of the reaction gas (CH_4/H_2) at the injection tube inlet are given to be 300 K and 2 m/sec, respectively.

v) The outflow boundary conditions are used at the reaction chamber exit.

B. Boundary conditions for species transport equations

i) The vanishing concentration gradients (zero fluxes) are imposed at the reaction chamber wall, symmetric axis, and chamber exit.

ii) At the torch exit, the only species existing in the plasma is assumed to be argon, *i.e.*, contributions of Ar^+ and e^- are neglected and charged species are not treated.

iii) The reaction gas composition at the injection tube inlet is kept constant as 5 % CH_4/95 % H_2.

Table 2. CH_4 and H_2 decomposition mechanism in argon thermal plasmas. A rate constant k of each forward reaction is expressed by $k = AT^n \exp(-E_a/RT)$, where units are given by kilocalories for E_a , Kelvin for T, and $R = 1.99 \times 10^{-3}$ kcal/mol deg.

Reactions	A	n	E_a
(R1) H + H + M = H_2 + M	9.7×10^{16}	-0.6	0.0
(R2) CH_3 + H + M = CH_4 + M	8.0×10^{26}	-3.0	0.0
(R3) CH_4 + H = CH_3 + H_2	2.2×10^{4}	3.0	8.8
(R4) CH_4 + CH_2 = CH_3 + CH_3	1.0×10^{13}	0.0	0.0
(R5) CH_3 + CH_3 = C_2H_5 + H	8.0×10^{14}	0.0	26.5
(R6) CH_3 + H = CH_2 + H_2	7.2×10^{14}	0.0	15.1
(R7) CH_3 + CH_2 = C_2H_4 + H	2.0×10^{13}	0.0	0.0
(R8) CH_3 + M = CH_2 + H + M	1.0×10^{16}	0.0	90.6
(R9) CH_2 + H = CH + H_2	4.0×10^{13}	0.0	0.0
(R10) CH + CH_4 = C_2H_4 + H	6.0×10^{13}	0.0	0.0
(R11) CH + CH_3 = C_2H_3 + H	3.0×10^{13}	0.0	0.0
(R12) C_2H_6 + H = C_2H_5 + H_2	5.4×10^{2}	3.5	5.2
(R13) C_2H_6 + CH_3 = C_2H_5 + CH_4	5.5×10^{-1}	4.0	8.3
(R14) C_2H_6 + M = CH_3 + CH_3 + M	1.0×10^{19}	0.0	68.0
(R15) C_2H_5 + M = C_2H_4 + H + M	1.0×10^{17}	0.0	31.0
(R16) C_2H_5 + CH_3 = C_2H_4 + CH_4	7.9×10^{11}	0.0	0.0
(R17) C_2H_4 + M = C_2H_2 + H_2 + M	2.6×10^{17}	0.0	79.4
(R18) C_2H_4 + M = C_2H_3 + H + M	2.6×10^{17}	0.0	96.6
(R19) C_2H_4 + H = C_2H_3 + H_2	1.5×10^{14}	0.0	10.2
(R20) C_2H_4 + CH_3 = CH_4 + C_2H_3	4.2×10^{11}	0.0	11.2
(R21) C_2H_3 + H = C_2H_2 + H_2	2.0×10^{13}	0.0	0.0
(R22) C_2H_3 + M = C_2H_2 + H + M	3.0×10^{15}	0.0	32.0
(R23) C_2H_3 + CH_3 = C_2H_2 + CH_4	7.9×10^{11}	0.0	0.0
(R24) C_2H_2 + M = C_2H + H + M	4.0×10^{16}	0.0	107.0
(R25) C_2H_2 + H = C_2H + H_2	6.0×10^{13}	0.0	23.7

5. Numerical method

The partial differential equations subject to boundary conditions and temperature-dependent plasma properties are solved by a control volume method using a semi-implicit pressure linked equations (SIMPLE) algorithm [8]. To improve the stability in the numerical computation, the analysis is accomplished by the following procedure. In the first step, only Ar, CH_4, and H_2 are considered without chemical reactions to determine the mixing temperature and main stream flow patterns inside the reaction chamber from the given boundary conditions. And then, when the main stream flow and temperature patterns are established, the chemical kinetic equations, involving 13 species and 25 reactions, are solved in the second step to obtain the concentration fields of all chemical species considered in the CH_4 decomposition process. Therefore, the computation is not fully self-consistent, since the temperature and flow fields are not re-calculated after the second step. However, such a computation procedure is not expected to lead the calculated results to any considerable discrepancies, because the developed main stream plasma fields would not be greatly altered not only by the chemical reactions but also by any changes in concentrations of reaction products determined in the second step. The computational domain used in this numerical work is described in Fig. 2.

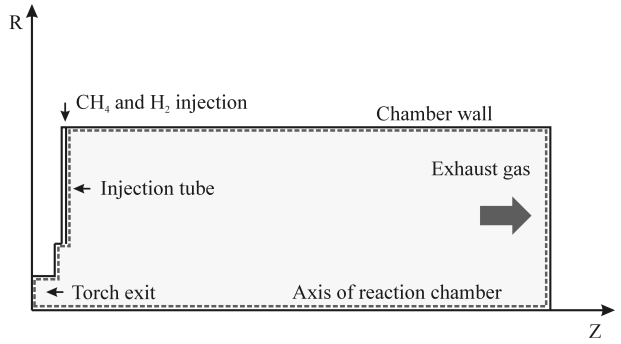

Fig. 2. Computational domain for a numerical analysis on the decomposition of CH_4 and H_2 in an argon thermal plasma.

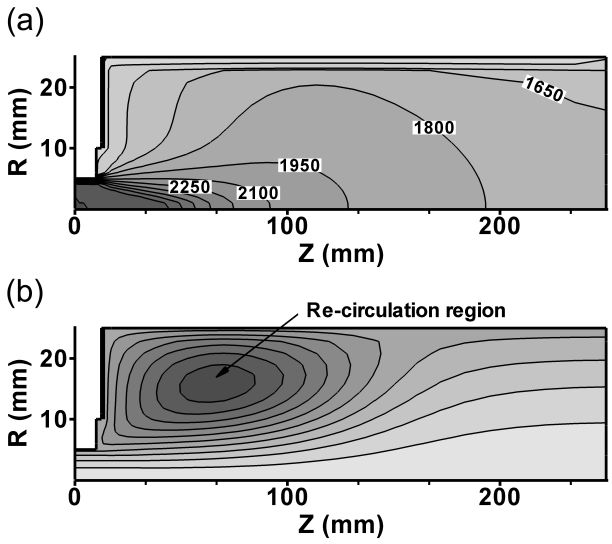

Fig. 3. Plasma temperature and flow patterns developed inside a reaction chamber; iso-contours of (a) the plasma temperature and (b) streamlines. The temperature difference between the iso-contours is 150 °K.

III. NUMERICAL RESULTS AND DISCUSSIONS

A complete description of temperatures and streamlines developed inside the reaction chamber is presented in Fig. 3. As shown in Fig. 3(a), the influx of reaction gases from the injection tube leads to a rapid cooling of the plasma temperature, and the temperature between 1500 °K and 2000 °K prevails in most parts of the reaction chamber. This estimated plasma temperature is well within a range of typical operation conditions of arc-jet diamond CVD processes. The streamlines in Fig. 3(b) show an existence of a large re-circulation region near the corner between the injection tube and reaction chamber wall. This re-circulating flow, which is originated from an abrupt change in diameter of the reaction chamber, enhances turbulent effects on the plasma jet, and expands the high temperature region toward the reaction chamber wall. As a result, a rapid cooling of the plasma jet temperature and a strong reduction of jet velocity occur, and steep gradients in the plasma temperature and velocity are established along the axis of the reaction chamber as seen in Fig. 4.

The calculated concentration fields of CH_3, H and C_2H_6, which are major reaction products in the diamond CVD, are drawn in terms of their mole fractions in Fig. 5, respectively. The reaction gases injected along the injection tube are effectively forced into the vicinity of the chamber centerline. However, the high-velocity stream of thermal plasma jet prevents the reaction gases from penetrating into the plasma jet. Therefore, it is found in Fig. 5(a)-(b) that the injected reaction gases of CH_4 and H_2 are mainly decomposed into CH_3 and H radicals in a peripheral region of the plasma jet flame. The concentrations of CH_3 and H show the relatively higher values around the discharged plasma jet. On the other hand, the concentration of C_2H_6, which is one of the main stable reaction products in the hydrocarbon decomposition process, shows somewhat different trends in its distribution, and increases in its absolute value toward the reaction chamber wall. Due to the large re-circulating flow in the reaction chamber, the part of generated radicals are stacked at the corner of the reaction chamber, where the temperature is very low, and begin to recombine into the stable species such as C_2H_6. Thus, the generation of C_2H_6 becomes active near the chamber wall than any other part of the reaction chamber. This is why the calculated mole fraction of C_2H_6 has the gradually increasing values toward the corner of the reaction chamber as appeared in Fig. 5(c).

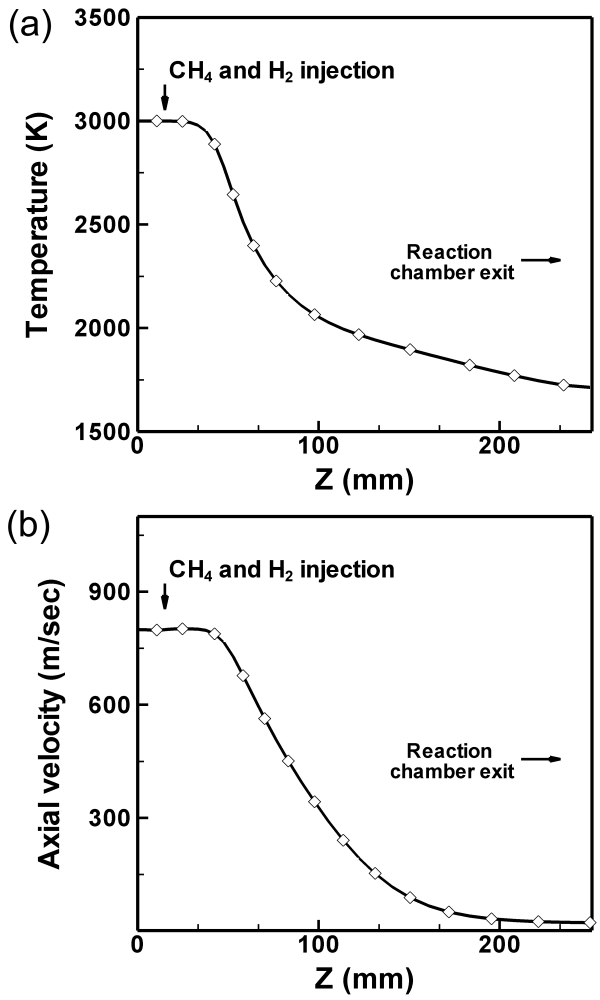

Fig. 4. Calculated plasma temperature and axial velocity profiles along the axis of a cylindrical reaction chamber; (a) plasma temperature and (b) axial velocity profiles.

With the absolute values of species concentrations in the reaction chamber, radial concentration profiles of the generated species are also important issues in actual diamond CVD processes, because they directly affect the

uniformity of synthesized diamond films. Therefore, radial concentration profiles of the major radicals such as CH_3 and H are investigated at different axial positions to see their position dependencies. The calculated profiles of each radical are plotted in Fig. 6 for three different axial positions, *i.e.*, Z = 30, 70, 150 mm. At Z = 30 mm, the concentration fields of both CH_3 and H radicals show the off-axis peaked profiles, *i.e.*, low density in the center of the plasma jet and high density around the plasma boundary. This can be easily understood from the previous discussion on the streamlines. As the distance from the torch exit increases, the centrally peaked profiles are gradually established and the peak values of the concentration reach their maximum values near the axial position of Z = 70 mm, where the reaction gases are highly dissociated. Finally, the radial profiles become nearly uniform as the distance increases further, and their shapes are almost flat at the axial position of Z = 150 mm. However, the absolute values of the concentrations of the effective radicals are considerably reduced. Thus it seems that the axial position has significant effects on the radial concentration characteristics such as uniformity and absolute values of concentration. In the thermal plasma diamond CVD, uniform

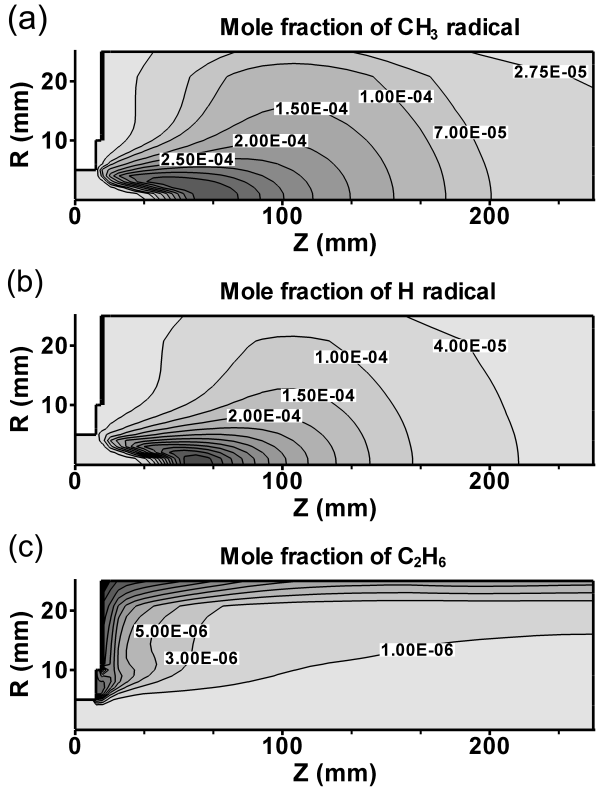

Fig. 5. Calculated mole fractions of major reaction products inside a reaction chamber; (a) methyl radical (b) hydrogen atom, and (c) ethane. The differences between the iso-contours are 0.5×10^{-4} for methyl radical and hydrogen atom, and 2.0×10^{-6} for ethane, respectively.

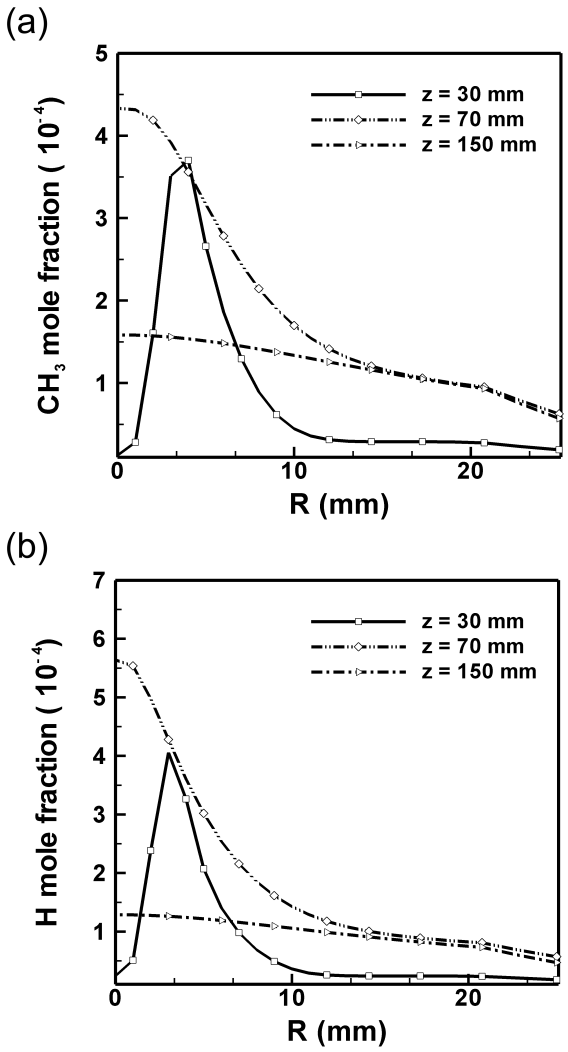

Fig. 6. Predicted radial profiles of major radicals mole fractions at various axial positions (Z = 30, 70, 150 mm); (a) methyl radical and (b) hydrogen atom.

plasmas abundant in reactive radicals are preferred as a favorable process environment, and a proper position of a substrate which ensures a good uniformity with reasonable growth rates must be determined in the process design stage. From the results of the present numerical work, it can be inferred that determination of the optimum process conditions can be easily accomplished by considering the radial transports of reaction products in the thermal plasma diamond CVD modeling.

Finally, mole fractions of all species considered in this work are calculated along the axis of the reaction chamber and their calculated results are presented in Fig. 7. From the presented plot, it is clearly seen that only several percents of CH_4 and H_2 fed into the reaction chamber are dissociated, and CH_3 is a primary diamond growth precursor. In addition, the calculation results illustrate that generations of stable reaction products, such as C_2H_2, C_2H_4 and C_2H_6, are not active along the

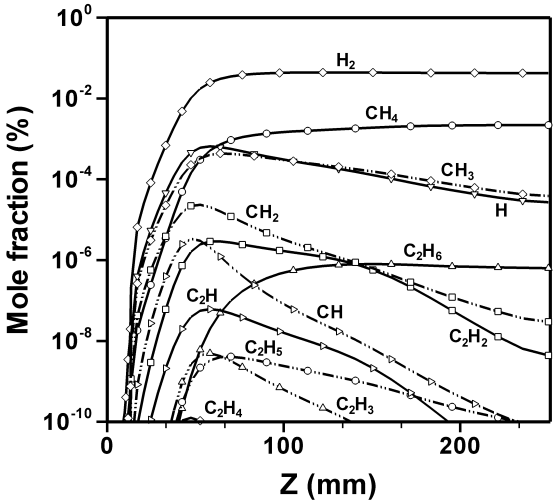

Fig. 7. Predicted axial profiles of mole fractions for all reaction products along the axis of a reaction chamber for the decomposition of CH_4 and H_2 by Ar thermal plasma

centerline of the reaction chamber, since the background temperature is rather high, *i.e.*, $T > 1700$ °K, and the dissociation of the stable reaction products is dominant in this temperature range.

IV. CONCLUSIONS

In the present numerical work, a 2D numerical analysis on a dc arc-jet diamond CVD process is performed to find out the effects of plasma fields on the production rates of CH_3 and H radicals during a CH_4/H_2 decomposition process. In the numerical calculation, the 2D approach successfully describes the physical phenomena such as re-circulating flows, mixing effects of reaction gases, and radial transports of reaction products. As a result, the strong effects of the thermal plasma jet fields on the concentration fields of the major reaction products are identified from the calculation results.

ACKNOWLEDGMENTS

This work has been supported by the Korea Institute of Science and Technology Evaluation and Planning (KISTEP) in Korea.

REFERENCES

[1] D. G. Goodwin, Appl. Phys. Lett. **59**, 277 (1991).
[2] D. F. Bahr, D. V. Bucci, L. S. Schadler, J. A. Last, J. Heberlein, E. Pfender and W. W. Gerberich, Diamond and Related Materials **5**, 1462 (1996).
[3] S. W. Reeve, W. A. Weimer and D. S. Dandy, J. Mater. Res. **11**, 694 (1996).
[4] M. Frenklach, J. Appl. Phys. **65**, 5142 (1989).
[5] M. I. Boulos, IEEE Trans. Plasma Sci. **19**, 1078 (1991).
[6] P. Fauchais and A. Vardelle, IEEE Trans. Plasma Sci. **25**, 1258 (1997).
[7] J. H. Park and S. H. Hong, J. Korean Phys. Soc. **31**, 753 (1997)
[8] S. V. Patankar, *Numerical Heat Transfer and Fluid Flow* (Hemisphere, New York, 1980).
[9] R. J. Kee, F. M. Rupley, E. Meeks and J. A. Miller, Sandia National Laboratories Report SAND96-8216 (1996).
[10] S. J. Harris, J. Appl. Phys. **65**, 3044 (1989).
[11] D. B. Olson and W. C. Gardiner, Combust. Flame **32**, 151 (1978).
[12] W. C. Gardiner, *Combustion Chemistry* (Springer, New York, 1984).
[13] P. Glarborg, J. A. Miller and R. J. Kee, Combust. Flame **65**, 177 (1986).
[14] W. J. Pitz and C. K. Westbrook, Combust. Flame **63**, 113 (1986).